Supporting Information for "Effect of dilatancy on the transition from aseismic to seismic slip due to fluid injection in a fault"

F. Ciardo[1]and B. Lecampion[1]

[1]Geo-Energy Laboratory, Gaznat chair on Geo-Energy,

École Polytechnique Fédérale de Lausanne, EPFL-ENAC-IIC-GEL, Switzerland.

Verification of the numerical scheme: benchmark for the non-dilatant case

The governing problem is uncoupled when elasticity does not affect fluid flow along the fault and vice-versa. This scenario occurs for a non dilatant fault, i.e. when the fault hydraulic aperture does not change during crack propagation, i.e. $w_h = \omega_o$. The pore pressure evolution in such a case is given by the solution of the linear diffusion equation in a fault characterized by constant hydraulic diffusivity $\alpha = \dfrac{k_f}{\mu\beta}$ [*Carslaw and Jaeger*, 1959]:

$$p\left(x,t\right) = p_o + \Delta P \cdot \mathrm{Erfc}\left|\frac{x}{\sqrt{4\alpha t}}\right| \tag{1}$$

This pore pressure evolution along the fault is linked to elasticity through the shear weakening Mohr-Coulomb criterion (one way coupling): the change of local effective normal stress associated with pore pressure increment reduces locally the fault frictional strength, affecting in turn elasticity.

Corresponding author: Brice Lecampion, brice.lecampion@epfl.ch

Garagash and Germanovich [2012] investigated extensively this particular case. Semi-analytical results are thus available, allowing to verify the numerical scheme. This is of great importance for these kind of non-linear (coupled) problems. Indeed, the dynamic instability that may occur during shear crack propagation due to weakening nature of friction coefficient may lead to numerical errors.

We show in Figure S1 the benchmark of our numerical results against the semi-analytical ones of *Garagash and Germanovich* [2012], both in terms of dimensionless half-crack length a/a_w and dimensionless peak slip accumulated in the middle of the fault $\delta_{|x=0}/\delta_w$. Notably, we chose three scenarios by changing the stress criticality τ_o/τ_p, while keeping a moderate over-pressure $\dfrac{\Delta P}{\sigma'_o} = 0.5$ and a friction weakening ration of $f_r/f_p = 0.6$, in order to test the numerical solver for different regimes of propagation: i) purely aseismic slip ($\tau_o/\tau_p = 0.51$), ii) aseismic crack propagation with nucleation and arrest of dynamic event ($\tau_o/\tau_p = 0.555$) and iii) aseismic slip followed by an unabated dynamic rupture ($\tau_o/\tau_p = 0.75$). We can observe in Figure S1 that our numerical results match perfectly with the semi-analytical ones of *Garagash and Germanovich* [2012]. The discrepancy in terms of half-crack length a/a_w between the numerical solutions and the semi-analytical ones is of the order of the element size h, the latter adopted such to have 25 elements within the frictional weakening zone (i.e. $a_w/h = 25$ - see the mesh convergence study reported in the following pages for relative error estimation). In Figure S2, the benchmark in terms of normalized slip δ/δ_w and shear stress τ/τ_p profile is reported (only for the case of aseismic crack propagation with nucleation and arrest of dynamic event). Again, we observe that the numerical results match the semi-analytical results of *Garagash and Germanovich* [2012] with good accuracy.

All the numerical results in terms of time evolution of half crack length a/a_w show a step-like behavior. This is intrinsically related to the modeling of the fault as a sum of adjacent finite elements of equal size h. Indeed, in one increment of time, the pore pressure perturbation might not be enough to activate further elements - i.e. to induce $F(\tau, \sigma'_n) = 0$. Time-stepping management as well as mesh resolution play an important role on this kind of step-like crack propagation. For a given increment of time Δt, the finer is the mesh the smaller are these steps. A local dynamic mesh refinement at the crack tips can reduce significantly this behavior, although the computational cost might considerably increase.

Mesh convergence study In order to check the accuracy of our numerical results, we have performed a mesh convergence study. Similarly to cohesive zone models for fracture propagation, the non linearity of the problem lies in a small zone near the crack tips. As already mentioned in section 2.1.2, such a small zone is approximately defined by the characteristic nucleation length-scale a_w, over which the friction coefficient weakens from a peak value to its residual value during crack propagation. It is of great importance, therefore, to have enough mesh resolution within that length-scale so as to be able to capture the non-linearity with good accuracy. A local dynamic mesh refinement at the crack tips can help in doing it, although the computational cost might considerably increase.

Since semi-analytical results of *Garagash and Germanovich* [2012] for non-dilatant frictional weakening fault are available, we have performed a mesh convergence study for the following test case: ultimately stable fault $\tau_o/\tau_p = 0.55$ (for a friction weakening ratio of $f_r/f_p = 0.6$), subjected to moderate overpressure $\dfrac{\Delta P}{\sigma'_o} = 0.5$ (and $\dfrac{\epsilon_d}{\beta\sigma'_o} = 0.$ - no dilatancy, uncoupled problem). Notably, we run bunch of simulations with the same initial configuration, while changing the total number of equal-sized elements (of size h) in a given mesh. The nucleation length-scale a_w is thus fixed for all the simulations (as it depends on friction weakening length-scale δ_w, initial stress conditions and elastic property of the medium, which are kept constant for all the simulations), while the element size h varies. In this way, we investigated the fault response in terms of half-crack length a/a_w and peak slip at the middle of the fault $\delta_{|x=0}/\delta_w$ as a function of the ratio a_w/h, which indicates the number of elements within the non-linear length-scale.

Figure S3 shows the relative error in terms of normalized peak slip $\delta_{|x=0}/\delta_w$ at a given normalized time $\sqrt{4\alpha t}/a_w = 2.$, between the numerical results and the semi-analytical

result of *Garagash and Germanovich* [2012], as a function of the number of elements within the nucleation length-scale a_w. We observe, not surprisingly, that the higher is the number of elements withing a_w, the lower is the relative error. For $a_w/h > 25$, the relative error is below 1%, up to reach 0.1% for $a_w/h = 50$. The non-monotonic decrease of the relative error for increasing values of a_w/h is related to step-like behavior of the numerical solutions that inevitably appear for low values of a_w/h (already discussed in section 1 of Supplemental Materials). This intrinsic behavior is, in fact, more pronounced for decreasing values of a_w/h, for which the accuracy deteriorates considerably.

Case of otherwise unstable fault $\tau_o > \tau_r$ - Nucleation and Arrest

In the case of zero dilatancy, for unstable fault with relatively low stress criticality, under moderate over-pressure (**region 4,b in Figure 3**), a finite seismic episode occurs prior to the nucleation of dynamic rupture. We investigate the effect of different dilatancy in such a configuration ($\tau_o/\tau_p = 0.65$, $\Delta P/\sigma'_o = 0.5$, $f_r/f_p = 0.6$). Figure S4 displays the time evolution of crack length and peak slip for different level of dilatancy.

Interestingly, the 'transient' seismic episode which is linked to the fact that the fluid front is initially ahead of the slipping patch (see **Figure S5** - comparison between pore pressure and slip profile at $\sqrt{4\alpha t}/a_w = 0.5$) does not disappear even for a dilatancy larger than the theoretical critical value $\epsilon_{d,c}/\beta\sigma'_o = 1/12$ in this case. Indeed such a seismic episode occurs with little accumulated slip and its nucleation is not influenced by residual friction: in such cases, the maximum dilatancy is not mobilized and no undrained strengthening of the fault occur. This can well be grasped by looking at the pore pressure profiles in **Figure S5** at dimensionless time $\sqrt{4\alpha t}/a_w = 1$, i.e. at a given time after the arrest of the seismic episode. The pore pressure drop is not fully developed due to the limited slip rate associated with crack propagation. However, the subsequent re-nucleation is increasingly delayed as the dilatancy increases (see **Figure S4** for $\frac{\epsilon_d}{\beta\sigma'_o} = 0.05$) and do not occur for values of dilatancy equal of above the critical value (case of $\frac{\epsilon_d}{\beta\sigma'_o} = 1/10$). Note that for such configurations, the nucleation of the unabated dynamic rupture occurs when a significant portion of the crack size is at residual friction, the weakening zone is small and confined near the tip (see friction coefficient profile in **Figure S5** at $\sqrt{4\alpha t}/a_w = 2.2$ - case of $\frac{\epsilon_d}{\beta\sigma'_o} = 0.05$). In such cases, the s.s.y assumption is valid,

the maximum dilatancy is active and the theoretical estimate for the critical dilatancy / undrained shear strength is valid.

Case of an ultimately stable fault even without dilatancy ($\tau_o < \tau_r$)

Normalized pressure, slip, friction & effective stress profiles

Dilatancy effect on purely aseismic crack propagation

Approximated solution for quasi-static growth assuming $a \propto \sqrt{4\alpha t}$

The numerical results showed in section 5.1 and 5.2 suggest that when the shear crack propagation is stable for large crack length, it appears to be synchronized with the fluid front position: i.e. $a = \gamma\sqrt{4\alpha t}$ for $a \gg a_w$ - at least for the constant permeability case. Following the approximated small scale yielding solution obtained for the non-dilatant case [*Garagash and Germanovich*, 2012], we make some further assumptions in order to extend it to account for dilatancy. The main difficulty lies in the determination of the pore-pressure changes in the dilatant case. With an approximated pore-pressure perturbation solution in hand, we can use the small scale yielding approximation of the fracture energy (23) and the expression of the stress intensity factor (25) to estimate γ from the quasi-static propagation condition.

We make from the onset the hypothesis that $a = \gamma\sqrt{4\alpha t}$, and that the permeability remains constant with slip. We further assume that the increment of hydraulic width with dilatancy is rather small such that $wk_f \approx w_o k_f$. In other words, we assume the fault hydraulic conductivity to remain constant. Under the small scale yielding approximation, we approximate the sink term due to dilatancy by two moving sink of intensity ϵ_d at the crack tips.

By scaling the variables of equation (14) with the following characteristic scales

$$\Pi = \tfrac{p(x,t)}{\Delta P}, \quad \xi = \tfrac{x}{\ell_d(t)}, \quad \gamma = \tfrac{a}{\ell_d(t)}$$

where $\ell_d = \sqrt{4\alpha t}$, the fluid flow equation reduces to the following ODE when γ is assumed to remain constant

$$-\frac{1}{4}\frac{\partial^2\Pi}{\partial\xi^2} - \frac{1}{2}\xi\frac{\partial\Pi}{\partial\xi} + \frac{1}{2}\xi \cdot \frac{\epsilon_d}{\beta \cdot \Delta P} \cdot \left(\delta_{dirac}\left(\xi - \gamma\right) + \delta_{dirac}\left(\xi + \gamma\right)\right) = 0 \tag{2}$$

We note in the previous equation (2) the presence of two moving sink terms that represent the undrained fault response occurring at small end zone of crack tips. With the following dimensionless boundary conditions

$$\Pi\left(0\right)=1, \qquad \Pi\left(\infty\right)=0, \tag{3}$$

equation (2) can be solved analytically:

$$\Pi(\xi,\gamma)=1-\mathrm{Erf}(\xi)-e^{\gamma^2}\sqrt{\pi}\gamma\Gamma_d\cdot$$
$$\left(-\mathrm{Erf}(\gamma)\left(1+\mathrm{Erf}(\xi)\right)+\left(\mathrm{Erf}(\gamma)-\mathrm{Erf}(\xi)\right)\cdot H(-\gamma+\xi)+\left(\mathrm{Erf}(\gamma)+\mathrm{Erf}(\xi)\right)\cdot H(\gamma+\xi)\right), \tag{4}$$

where H is the Heaviside step function and $\Gamma_d=\dfrac{\epsilon_d}{\beta\cdot\Delta P}=\dfrac{\epsilon_d}{\beta\sigma'_o}\dfrac{\sigma'_o}{\Delta P}$ is a dimensionless parameter capturing the effect of the undrained pore pressure drop with respect to the injection fluid over-pressure. Note that the dimensionless over-pressure at the tip simplify to:

$$\Pi(\gamma,\gamma)=\mathrm{Erfc}\left(\gamma\right)\left(1-\gamma\sqrt{\pi}\ \mathrm{e}^{\gamma^2}\Gamma_D\mathrm{Erf}\left(\gamma\right)\right) \tag{5}$$

Equation (4) thus allows to calculate analytically the SIF (through equation (25)):

$$K_{II}=\tau_p\sqrt{\ell_d}\times\left(\sqrt{\pi}\left(\frac{\tau_o}{\tau_p}-\frac{f_r}{f_p}\right)+\frac{f_r}{f_p}\frac{\Delta P}{\sigma'_o}\Delta k_{II}(\gamma,\Gamma_d)\right) \tag{6}$$
$$\Delta k_{II}(\gamma,\Gamma_d)=\sqrt{\pi}-\frac{4\gamma}{\pi}\left(1+\gamma\sqrt{\pi}\ \mathrm{e}^{\gamma^2}\Gamma_D\mathrm{Erfc}\left(\gamma\right)\right)\ {}_p\mathrm{F}_q(\{1/2,1\},\{3/2,3/2\},-\gamma^2) \tag{7}$$

where ${}_p\mathrm{F}_q$ denotes the generalized hypergeometric function. Note that interestingly, in the limit of large crack length (i.e. large $\gamma\ell_d$), we recover the exact same limit than the simpler approximation of the superposition of a point source with an uniform undrained pore-pressure drop used in section 3.2.2:

$$\lim_{a\to\infty}K_{II}=\infty\left(\tau_o-\frac{\epsilon_d}{\beta\sigma'_o}f_r-\tau_r\right)=\infty\left(\tau_o-\tau_r^u\right), \tag{8}$$

and therefore the same critical value of dilatancy (27) required to stabilize an otherwise unstable fault.

Under such a small scale yielding approximation, assuming that the over-pressure is uniform in the weakening zone and equal to its value at the crack tip, the fracture energy G_c (see eq. (23)) can be approximated as

$$G_c = (f_p - f_r)\frac{\delta_r \sigma'_o}{2}\left(1 - \frac{\Delta P}{\sigma'_o} \times \Pi(\gamma, \gamma)\right) \tag{9}$$

The quasi static propagation condition (24) can thus be re-written as:

$$\frac{a_w}{\ell_d}\left(\frac{f_p - f_r}{f_p}\right)^2 \left(1 - \frac{\Delta P}{\sigma'_o} \times \Pi(\gamma, \gamma)\right) = \left\{\sqrt{\pi}\left(\frac{\tau_o}{\tau_p} - \frac{f_r}{f_p}\right) + \frac{f_r}{f_p}\frac{\Delta P}{\sigma'_o}\Delta k_{ii}(\gamma, \Gamma_d)\right\}^2 \tag{10}$$

The previous equation can be solved for γ for a given set of problem parameters (τ_o/τ_p, f_r/f_p, $\Delta P/\sigma'_o$, $\epsilon_d/(\beta\sigma'_o)$) and a given value of a_w/ℓ_d. Although, we made the assumption of a time-independent γ to obtain the pore-pressure profile, we can relax it to see its evolution with a_w/ℓ_d. The obtained approximated solution captures the order of magnitude of the aseismic shear crack propagation as can be seen on Figure S8. However, it is not precise enough essentially due to i) the impact of the change of hydraulic conductivity with slip which prevent to properly captured the pore-pressure profile (as can be seen on Figure S9) and ii) the fact that the pore-pressure is clearly not uniform in the weakening zone which impact the estimation of the fracture energy in the small scale assumption.

Effect of shear-induced permeability changes: case of slip-dependent permeability

Normalized pressure, slip, friction & effective stress profiles.

Effect of shear-induced permeability changes: case of effective stress-dependent permeability

Time evolution of normalized half crack length & peak slip.

Normalized pressure, slip, friction & effective stress profiles.

Comparison between quasi-static and quasi-dynamic crack propagation on critically stressed dilatant fault

Time evolution of normalized half crack length & peak slip.

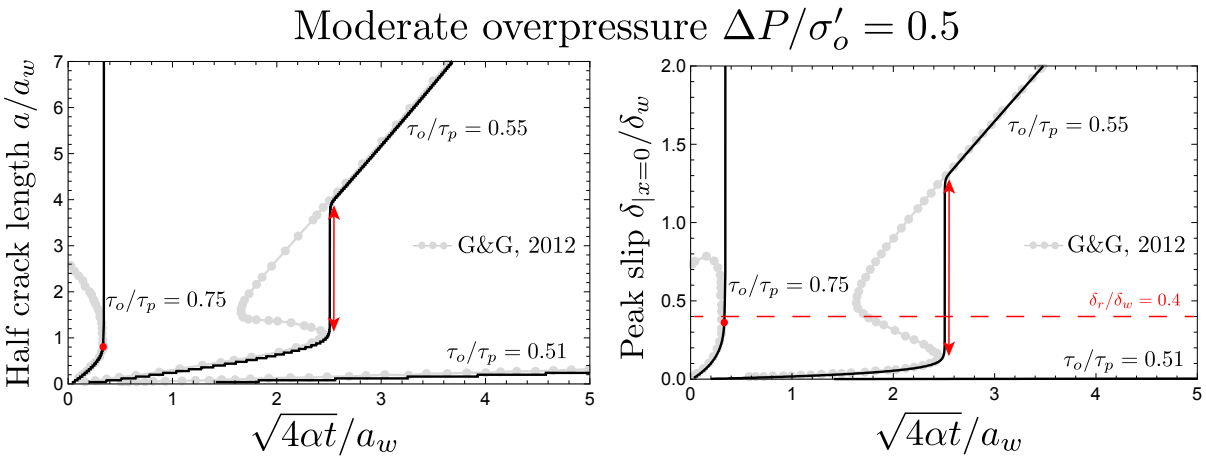

Figure S1. Benchmark of numerical results against semi-analytical ones of *Garagash and Germanovich* [2012] in terms of time evolution of normalized half crack length a/a_w and normalized peak slip δ/δ_w at $x = 0$, for a non-dilatant fault subjected to moderate overpressure $\Delta P/\sigma'_o = 0.5$ and three initial stress conditions: i) $\tau_o/\tau_p = 0.75$ (unstable fault), ii) $\tau_o/\tau_p = 0.55$ (ultimately stable fault) and iii) $\tau_o/\tau_p = 0.51$ (ultimately stable fault). The friction weakening ratio is $\dfrac{f_r}{f_p} = 0.6$, so that $\dfrac{\delta_r}{\delta_w} = 0.4$. The red dots denote the nucleation/onset of an unabated dynamic rupture, whereas the red arrows denote the nucleation of dynamic event followed by an arrest.

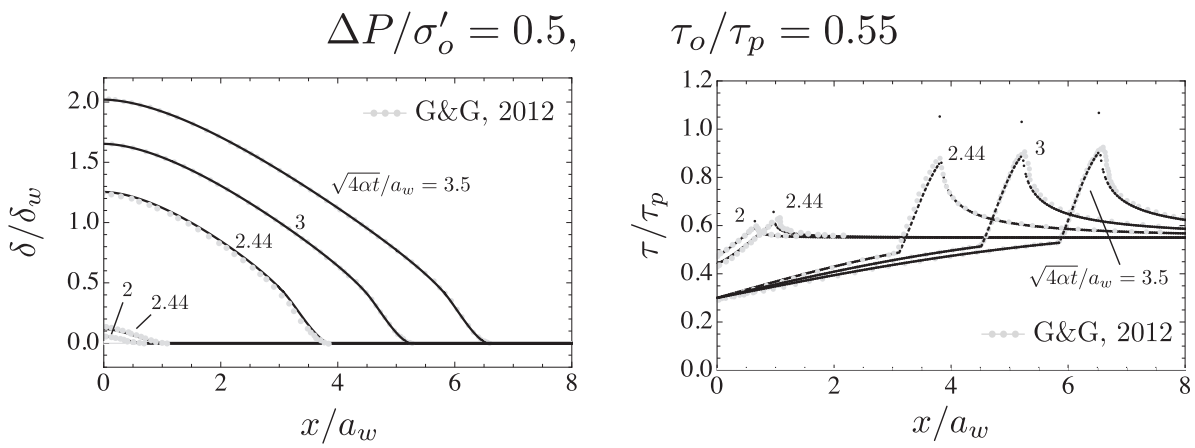

Figure S2. Benchmark of numerical results against semi-analytical ones of *Garagash and Germanovich* [2012] in terms of normalized slip δ/δ_w and shear stress τ/τ_p profiles, for a non-dilatant ultimately stable fault subjected to moderate over-pressure $\Delta P/\sigma'_o = 0.5$. The stress criticality is $\tau_o/\tau_p = 0.55$ and the friction weakening ratio is $f_r/f_p = 0.6$.

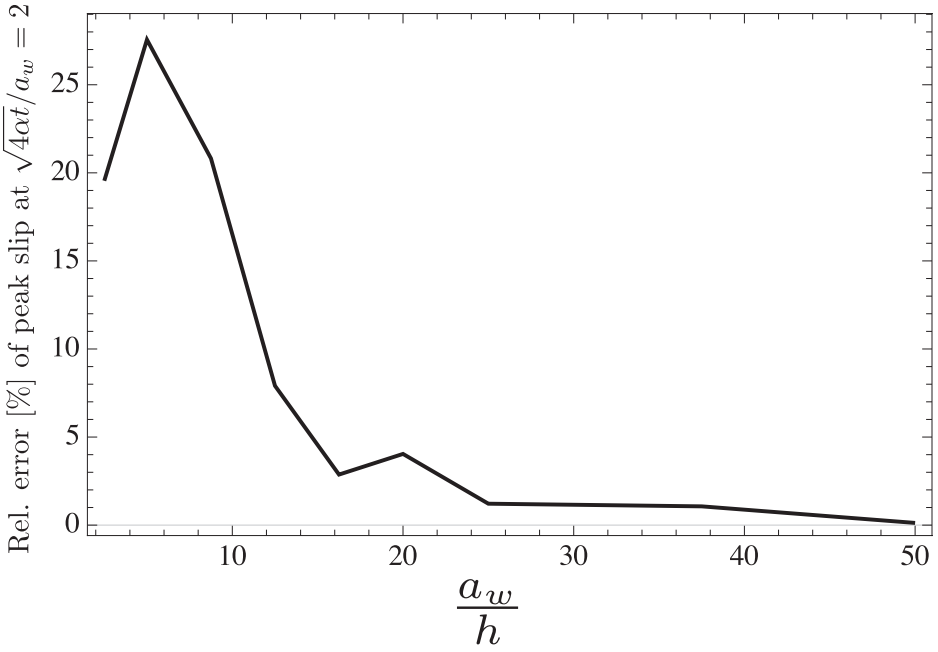

Figure S3. Evolution of relative error in terms of normalized peak slip $\delta_{|x=0}/\delta_w$ at normalized time $\sqrt{4\alpha t}/a_w = 2$, as a function of number of elements within the nucleation length scale a_w. The test case investigated is a non-dilatant ultimately stable fault ($\tau_o/\tau_p = 0.55$ and $f_r/f_p = 0.6$), subjected to moderate overpressure $\dfrac{\Delta P}{\sigma'_o} = 0.5$. Semi-analytical results of *Garagash and Germanovich* [2012] in terms of normalized half crack length and peak slip at the fault center are available, allowing to calculate the relative error.

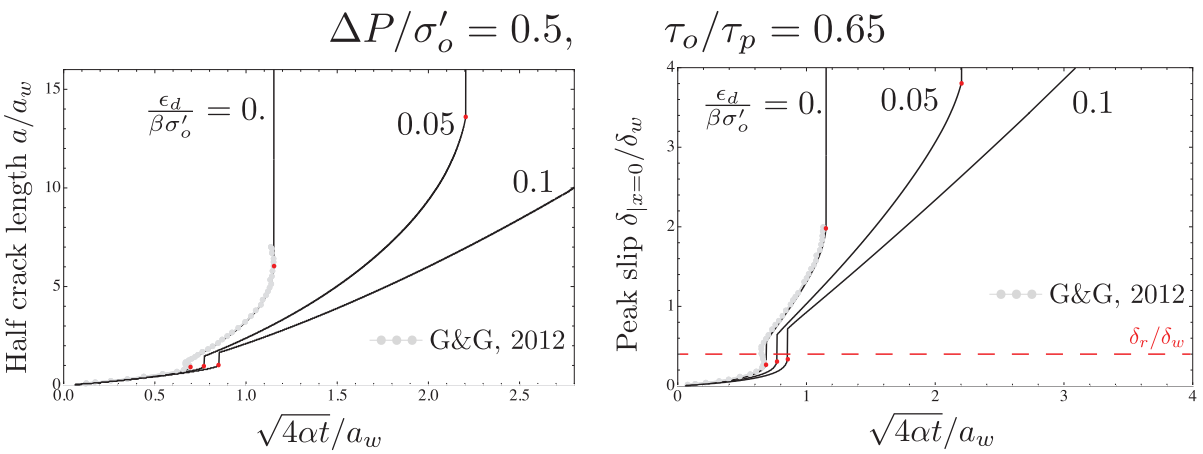

Figure S4. Evolution of normalized half crack length a/a_w and normalized peak slip $\delta_{|x=0}/\delta_w$ with normalized time $\sqrt{4\alpha t}/a_w$ for a frictional weakening dilatant fault. The fault is subjected to an initial uniform background shear stress $\tau_o/\tau_p = 0.65$ (unstable fault in the non-dilatant case for a friction weakening ratio of $f_r/f_p = 0.6$ - with relative low stress criticality though) and a moderate constant over-pressure $\dfrac{\Delta P}{\sigma'_o} = 0.5$ applied in the middle of the fault. Two dimensionless dilatancy parameters are considered: $\dfrac{\epsilon_d}{\beta\sigma'_o} = 0.05 < \dfrac{\tau_o}{\tau_r} - 1 = \dfrac{\epsilon_{d,c}}{\beta\sigma'_o}$ and $\dfrac{\epsilon_d}{\beta\sigma'_o} = 0.1 > \dfrac{\tau_o}{\tau_r} - 1 = \dfrac{\epsilon_{d,c}}{\beta\sigma'_o}$. Grey dotted lines denote semi-analytical results of *Garagash and Germanovich* [2012], whereas red dots denote nucleation of dynamic rupture.

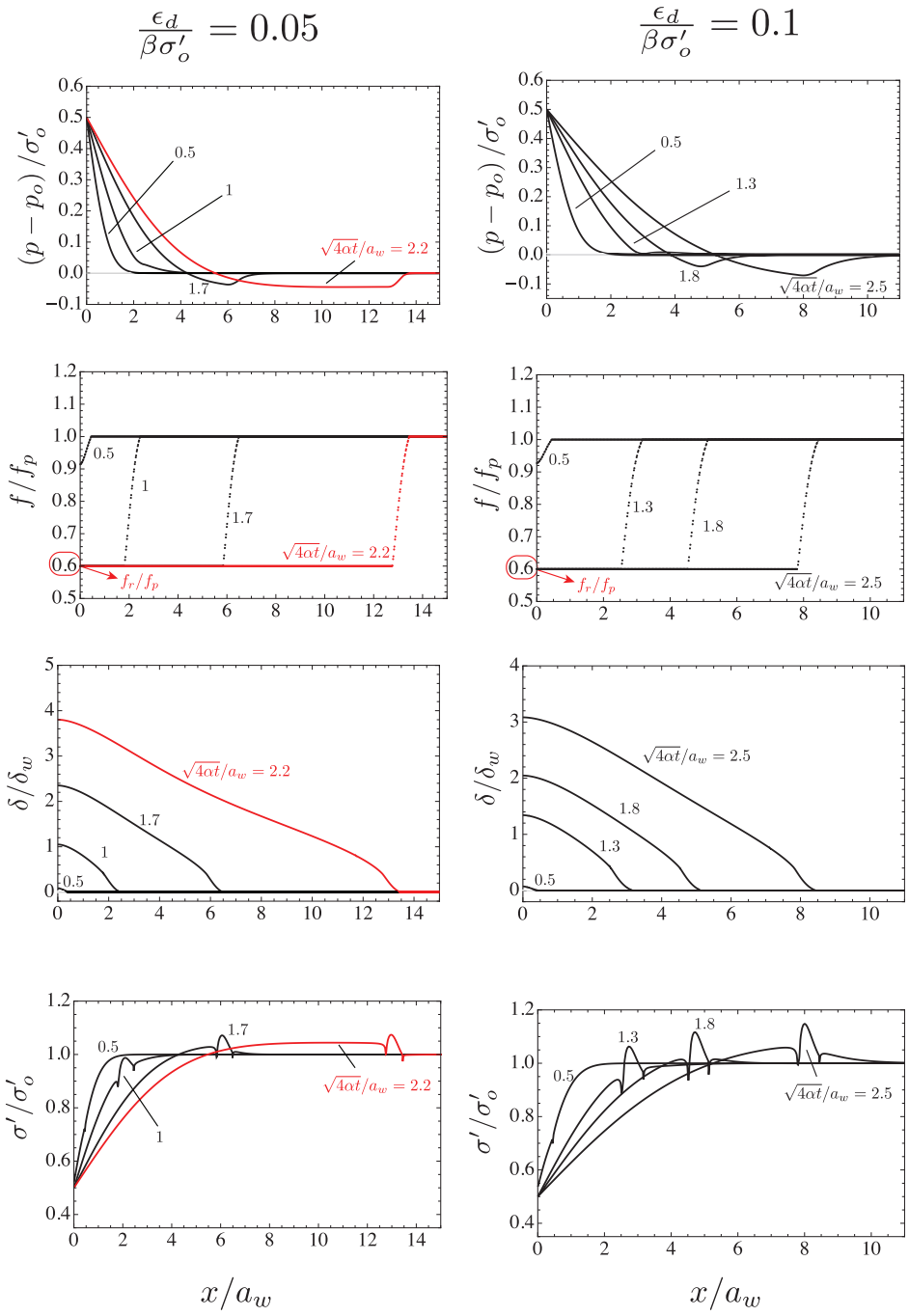

Figure S5. Spatial profiles of dimensionless pore pressure (a), friction coefficient (b), slip (c) and effective normal stress (d) at different (normalized) time snapshots, for an otherwise unstable fault ($\tau_o/\tau_p = 0.65$ - relative low stress criticality for $f_r/f_p = 0.6$), subjected to a moderate over-pressure $\frac{\Delta P}{\sigma'_o} = 0.5$. Two dimensionless dilatancy parameters are considered: $\frac{\epsilon_d}{\beta\sigma'_o} = 0.05 < \frac{\tau_o}{\tau_r} - 1 = \frac{\epsilon_{d,c}}{\beta\sigma'_o}$ and $\frac{\epsilon_d}{\beta\sigma'_o} = 0.1 > \frac{\tau_o}{\tau_r} - 1 = \frac{\epsilon_{d,c}}{\beta\sigma'_o}$. Red lines refer to numerical results at nucleation time of an unabated dynamic rupture.

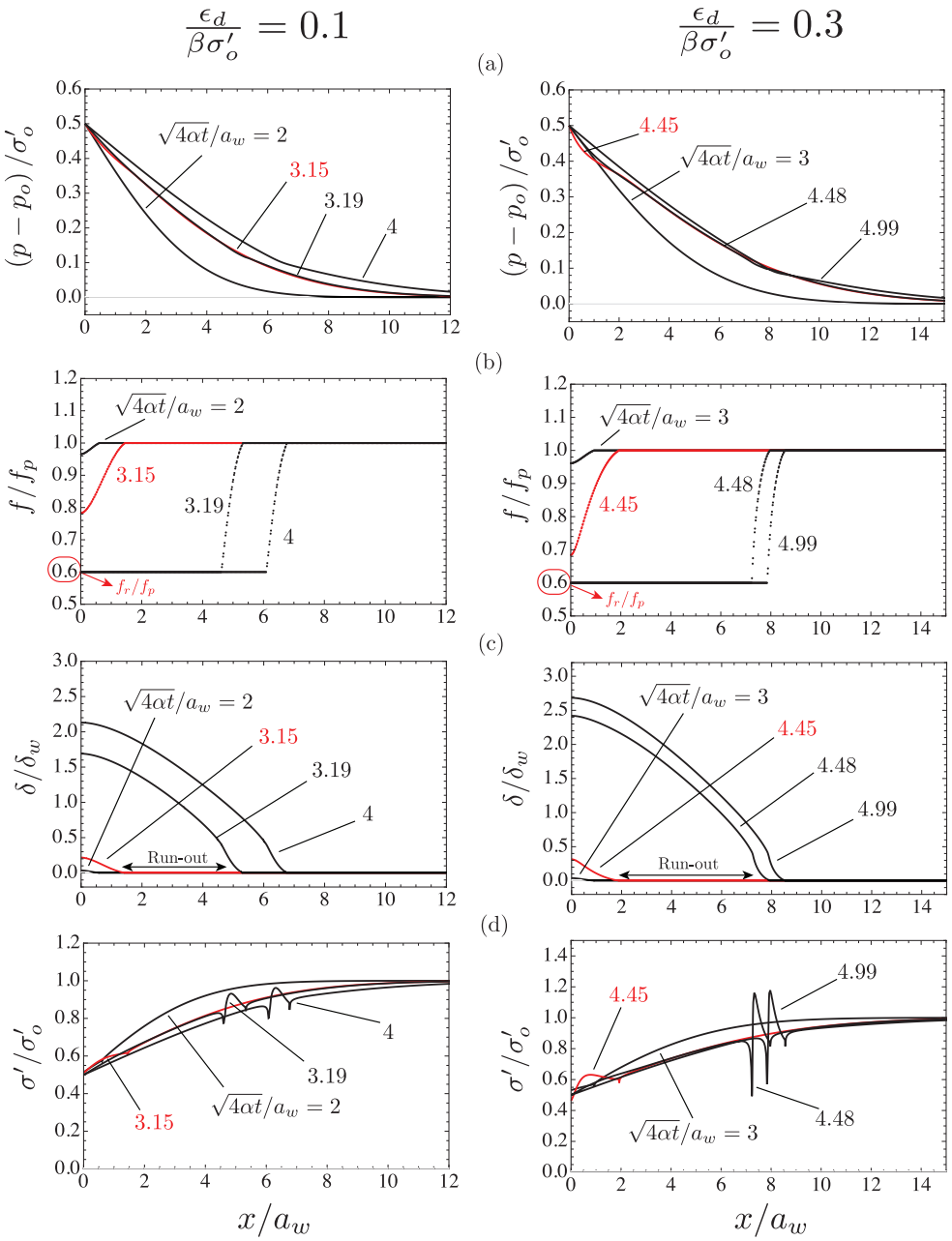

Figure S6. Spatial profiles of dimensionless pore pressure (a), friction coefficient (b), slip (c) and effective normal stress (d) at different (normalized) time snapshots, for an otherwise ultimately stable fault ($\tau_o/\tau_p = 0.55$ - $f_r/f_p = 0.6$), subjected to a moderate over-pressure $\frac{\Delta P}{\sigma'_o} = 0.5$. Two dimensionless dilatancy parameters are considered: $\frac{\epsilon_d}{\beta\sigma'_o} = 0.1$ and $\frac{\epsilon_d}{\beta\sigma'_o} = 0.3$. Red lines refer to numerical results at nucleation time of a dynamic rupture. Since the background shear stress τ_o is lower than the residual fault strength τ_r at ambient conditions, the dynamic event is always followed by an arrest.

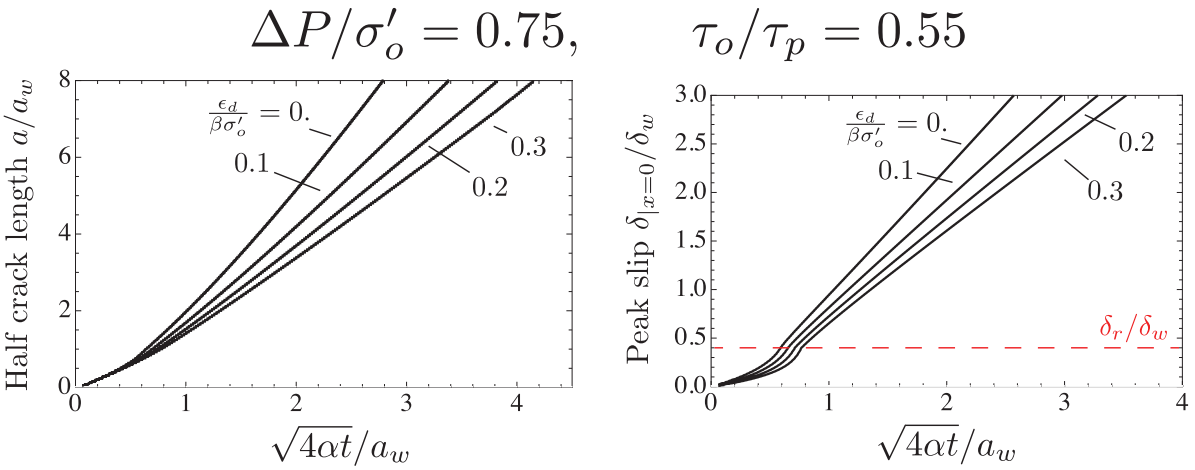

Figure S7. Dilatancy effect on normalized crack length a/a_w and peak slip δ/δ_w at $x = 0$ for a frictional weakening fault subjected to large overpressure $\Delta P/\sigma'_o = 0.75$. The fault is ultimately stable in the hypothetical absence of dilatancy as the uniform background shear stress $\tau_o = 0.55 \cdot \tau_p$ is lower than the fault residual strength at ambient conditions τ_r, for a friction weakening ratio of $f_r/f_p = 0.6$. Under such stress criticality and large over-pressure, the fault always exhibits seismic crack propagation (zone 3 of Figure 3). However, the crack velocity slows down for increasing values of dimensionless dilatancy parameters.

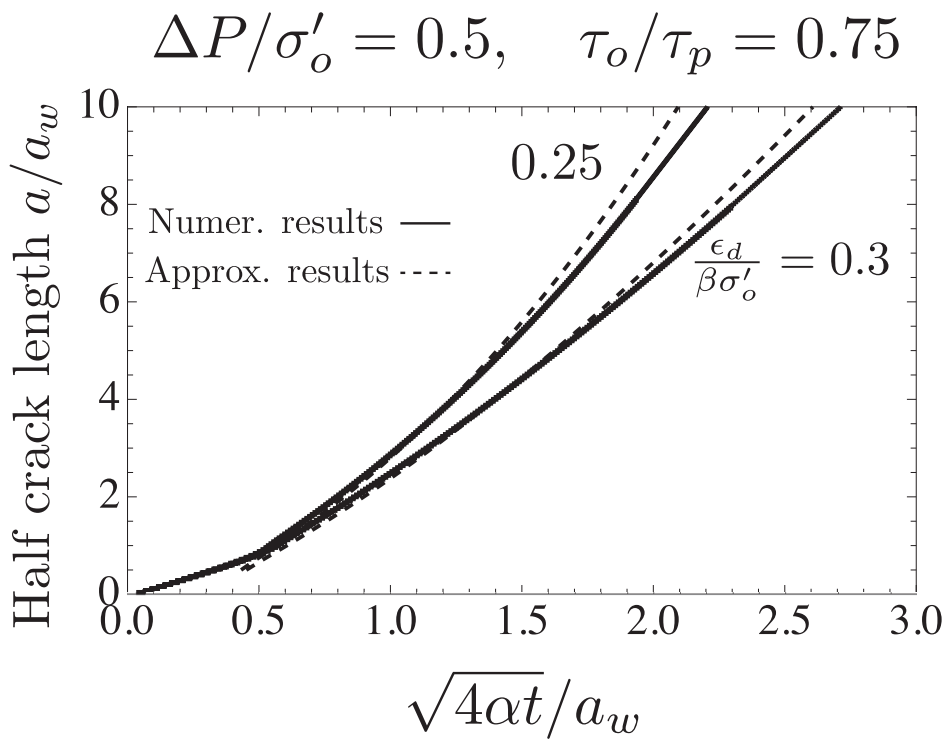

Figure S8. Comparison between numerical results and results associated with approximated solution for quasi-static crack growth ($a \propto \sqrt{4\alpha t}$) in terms of time evolution of normalized half-crack length a/a_w. The case investigated is a critically stressed fault ($\tau_o/\tau_p = 0.75$), subjected to moderate over-pressure $\Delta P/\sigma'_o = 0.5$ and two values of dimensionless dilatancy parameter $\frac{\epsilon_d}{\beta\sigma'_o} = 0.25 - 0.3$.

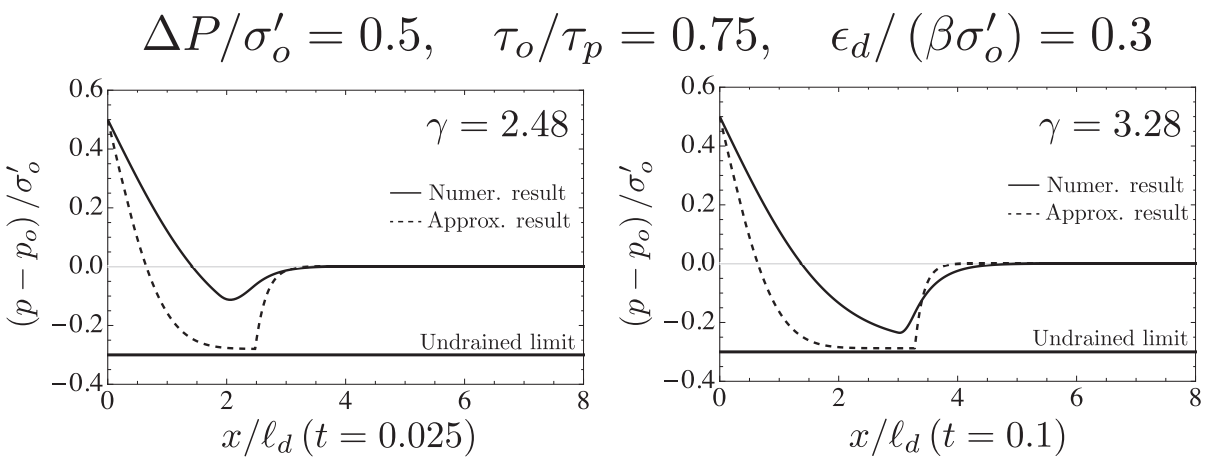

Figure S9. Comparison between numerical results and results associated with approximated solution for quasi-static crack growth ($a \propto \sqrt{4\alpha t}$) in terms of pore pressure profiles. The case investigated is a critically stressed fault ($\tau_o/\tau_p = 0.75$), subjected to moderate over-pressure $\Delta P/\sigma'_o = 0.5$ and a dimensionless dilatancy parameter $\dfrac{\epsilon_d}{\beta\sigma'_o} = 0.3$. The relative (and constant) position between crack tip and fluid front ($\gamma = \dfrac{a}{\ell_d(t)}$) is 2.48 and 3, which correspond to a dimensionless time of $\sqrt{4\alpha t}/a_w = 1$ and $\sqrt{4\alpha t}/a_w = 2$, respectively

.

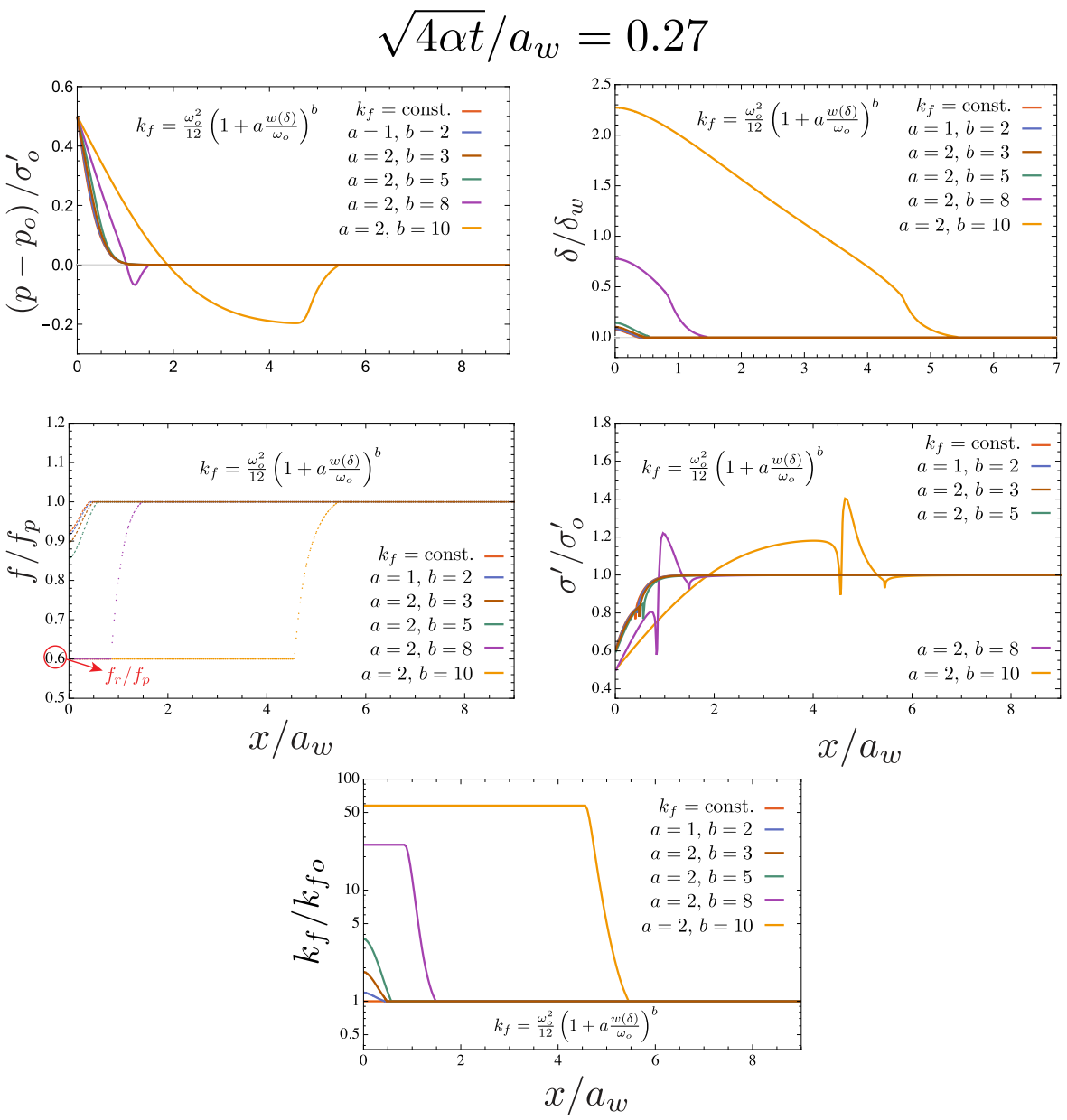

Figure S10. Spatial profiles of dimensionless pore pressure, friction coefficient, slip, effective normal stress and fault longitudinal permeability (in linear-log scale) at a given normalized time snapshot $\sqrt{4\alpha t}/a_w = 0.27$, for unstable fault ($\tau_o/\tau_p = 0.75$ - $f_r/f_p = 0.6$), subjected to a moderate over-pressure $\dfrac{\Delta P}{\sigma'_o} = 0.5$ and a dimensionless dilatancy parameter equal to the critical value, i.e. $\dfrac{\epsilon_{d,c}}{\beta\sigma'_o} = 0.25$. The different numerical results are obtained with different fault permeability evolution laws: i) constant permeability $k_f = \dfrac{\omega_o^2}{12}$, ii) slip-dependent permeability law $k_f = \dfrac{\omega_o^2}{12}\left(1+a\dfrac{w(\delta)}{\omega_o}\right)^b$, with $a = 1 \& b = 2$ (cubic law for fault transmissivity) and $a = 2 \& b = 3, 5, 8, 10$.

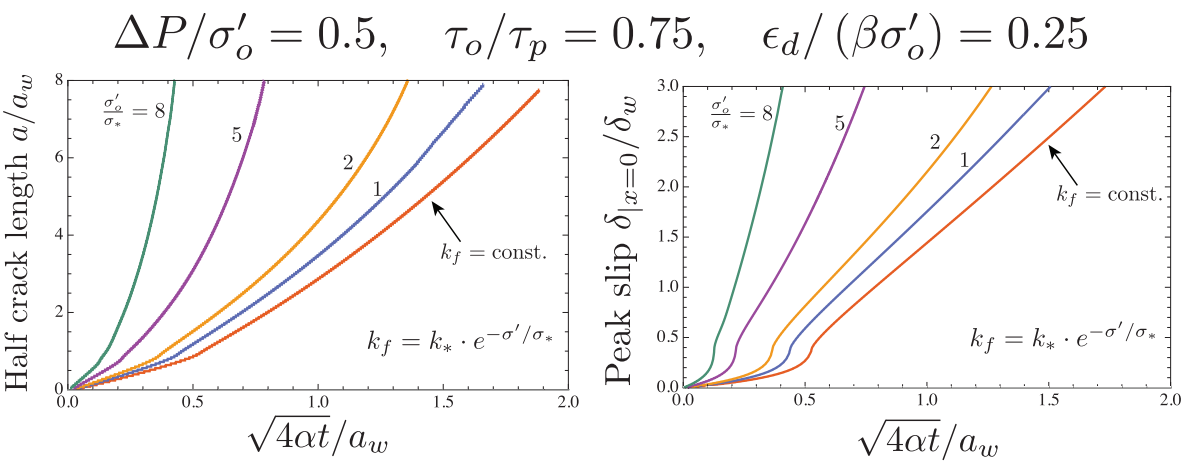

Figure S11. **Effect of permeability increase on a critically stressed ($\tau_o/\tau_p = 0.75$, $f_r/f_p = 0.6$) dilatant fault in terms of time evolution of normalized half crack length a/a_w and peak slip $\delta_{|x=0}/\delta_w$. The dimensionless dilatancy parameter $\epsilon_d/(\beta\sigma'_o)$ is taken here equal to the critical stabilizing value 0.25. Under such conditions a fault with constant fault permeability $k_f = \omega^2/12$, subjected to moderate overpressure $\Delta P/\sigma'_o = 0.5$, never exhibit seismic slip. An effective stress-dependent permeability law has been considered ($k_f = k_* e^{(-\sigma'/\sigma_*)}$), with four different ratios of σ'_o/σ_* spanning low and large permeability increase.**

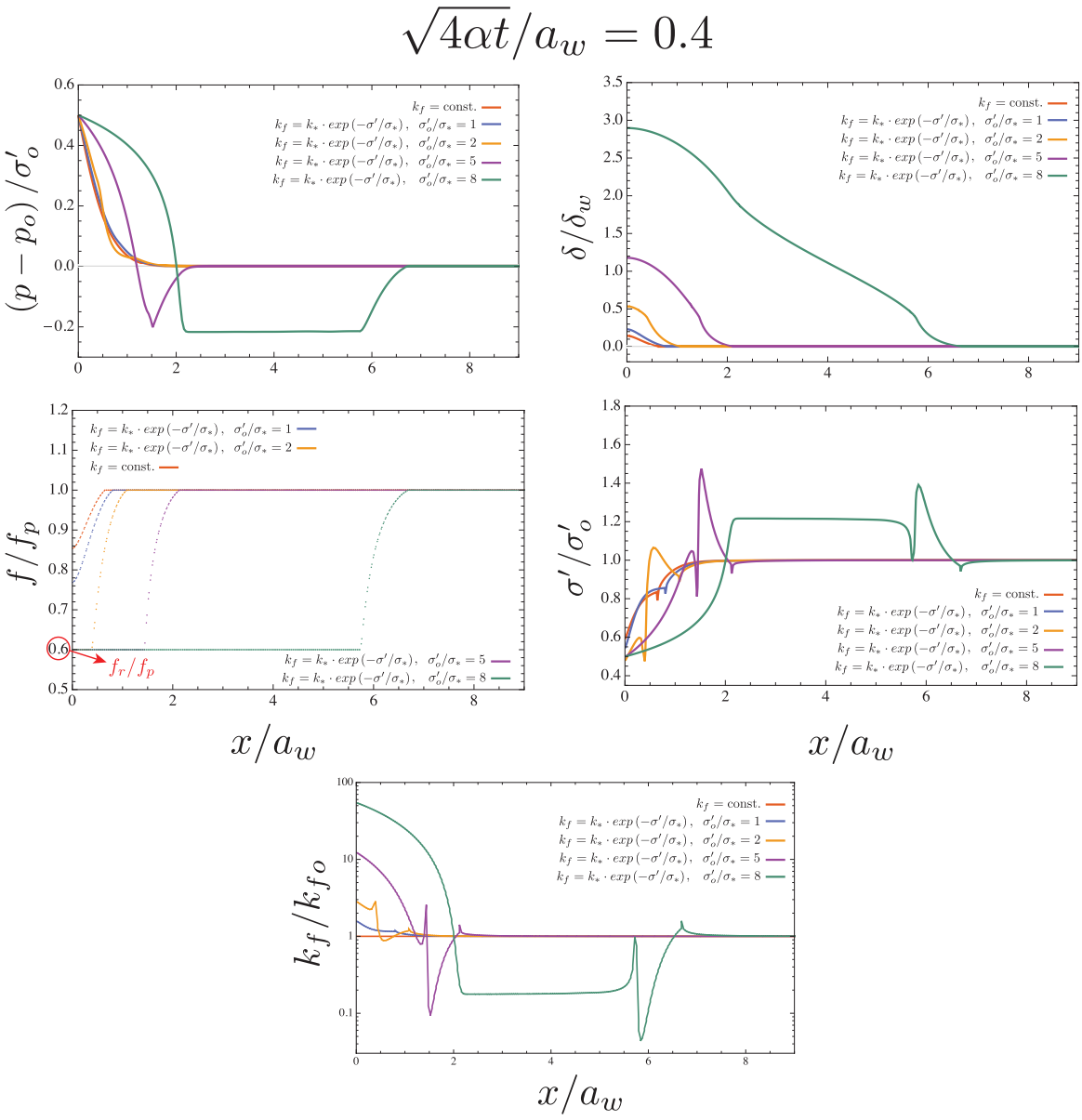

Figure S12. Spatial profiles of dimensionless pore pressure, friction coefficient, slip, effective normal stress and fault longitudinal permeability (in linear-log scale) at a given normalized time snapshot $\sqrt{4\alpha t}/a_w = 0.4$, for unstable fault ($\tau_o/\tau_p = 0.75$ - $f_r/f_p = 0.6$), subjected to a moderate over-pressure $\dfrac{\Delta P}{\sigma'_o} = 0.5$ and a dimensionless dilatancy parameter equal to the critical value, i.e. $\dfrac{\epsilon_{d,c}}{\beta\sigma'_o} = 0.25$. The different numerical results are obtained with different fault permeability evolution laws: i) constant permeability $k_f = \dfrac{\omega_o^2}{12}$, ii) effective stress-dependent permeability law $k_f = k_* \cdot e^{(-\sigma'/\sigma_*)}$, with $\sigma'_o/\sigma_* = 1 - 2 - 5 - 8$.

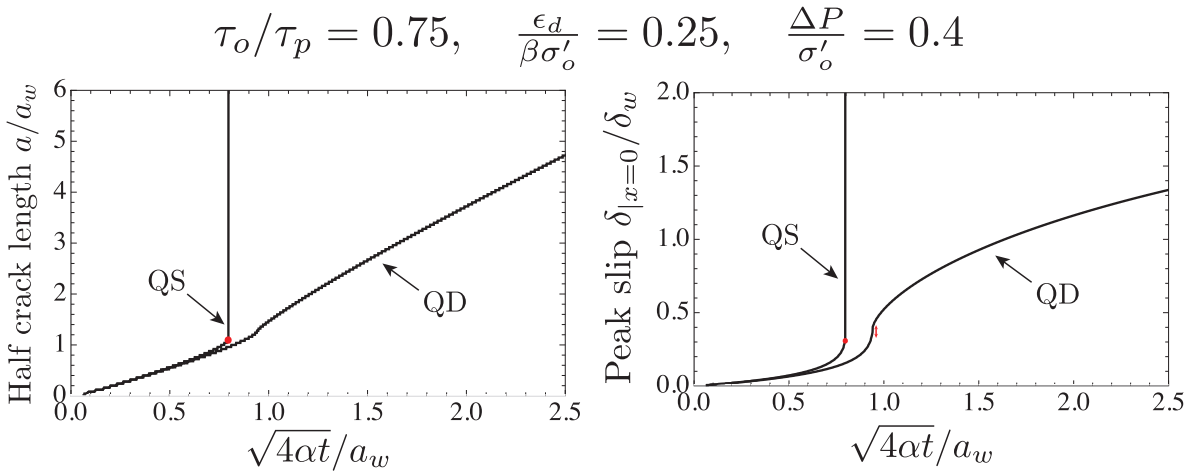

Figure S13. Time evolution of normalized half crack length and peak slip under quasi-static (QS) and quasi-dynamic (QD) approximation of elastic equilibrium. The latter is obtained by adding a seismic radiation damping term proportional to slip rate to elasticity equations in order to take into account energy dissipation through seismic waves orthogonal to fault plane during high slip rate [*Rice*, 1993]. The radiation damping term in normalized form reads $\frac{G\delta_w 4\alpha}{2c_s\tau_p a_w^2}$, being c_s the shear wave speed and G the shear modulus. We use here a very large value of 40 for such a dimensionless damping term, therefore over-damping the dynamic rupture.